



Crystallization of Mechanically Alloyed Ni₅₀Ti₅₀ and Ti₅₀Ni₂₅Cu₂₅ Shape Memory Alloys

Piotr Salwa and Tomasz Goryczka

(Submitted September 2, 2019; in revised form March 30, 2020; published online May 4, 2020)

The Ni₅₀Ti₅₀ and Ti₅₀Ni₂₅Cu₂₅ alloys were produced in the form of powder using the high-energy ball milling. In the as-milled state, both alloys revealed presence of an amorphous state with a small amount of nanocrystalline areas. The non-isothermal DSC heating curves were used to investigate the crystallization process. Temperatures and activation energy of crystallization were determined. In both alloys, the crystallization occurred at temperatures range from 777 to 813 K, dependently on the heating rate. The activation energy values determined by the Kissinger and Ozawa method were comparable for both alloys and ranged from 410 to 429 kJ/mol.

Keywords activation energy, crystallization, high-energy ball milling, NiTi, NiTiCu

1. Introduction

Parameters of manufacturing process, applied for alloys production, highly impact their structure. This effect is clearly visible when mechanical alloying is used, in which the material can be obtained in amorphous and/or nanocrystalline form. Shape memory effects do not occur in the amorphous state. However, the use of thermal treatment gives the possibility to shape the appropriate grain size. Thus, the shape memory effects can be controlled. Crystallization of amorphous materials is complex phenomenon due to nucleation and/or growth processes of residual precursor nuclei introduced into the alloy during either amorphization or due to impurities introduced through manufacturing method (Ref 1). Hence, understanding the crystallization process in amorphous alloys is crucial to controlling and/or obtaining a nanocrystalline or micrograins.

NiTi-based alloys can be obtained in amorphous state by various methods—repeated cold rolling (Ref 2), severe plastic deformation (Ref 3), high-pressure torsion (Ref 4), melt spinning (Ref 5) and mechanical alloying (Ref 6–8). Adjustment of parameters such as grinding time, grinding speed or ball-to-material ratio allows acquiring either amorphous alloy and/or alloy in nanocrystalline form. Specially, the nanocrystalline form gives the possibility to influence the course of the reversible martensitic transformation via controlling the grain size.

This article is an invited submission to JMEP selected from presentations at The XXII Physical Metallurgy and Materials Science Conference: Advanced Materials and Technologies (AMT 2019) held June 9–12, 2019, in Bukowina Tatrzańska, Poland, and has been expanded from the original presentation.

Piotr Salwa and Tomasz Goryczka, Institute of Materials Science, University of Silesia in Katowice, 75 Pułk Piechoty 1A, 41-500 Chorzow, Poland. Contact e-mail: salwa.piotr@gmail.com.

Therefore, in the presented work, we focused on a detailed analysis of the crystallization process taking place in amorphous Ni₅₀Ti₅₀ and Ti₅₀Ni₂₅Cu₂₅ alloys produced by high-energy ball milling, using non-isothermal approach. In the crystalline state, both alloys show the presence of the one-step reversible martensitic transformation; however, it differs in its final product: in the Ni₅₀Ti₅₀ alloy, the low-temperature phase is the B19' monoclinic martensite and in the case of Ti₅₀Ni₂₅Cu₂₅—the B19 orthorhombic one.

2. Materials and Methods

Commercially available nickel, titanium and copper elemental powders (Atlantic Equipment Engineers) of 99.7% purity were used for production of the Ni₅₀Ti₅₀ and Ti₅₀Ni₂₅Cu₂₅ alloys. First proper weighted powders of alloying elements were mixed for 48 h in Netzsh planetary mill. Then obtained mixtures were used as starting powders for high-energy ball milling. They were milled continuously for 100 h in a Fritsch Pulverisette 7 premium line planetary-ball mill at argon protective atmosphere. This procedure was carried out with 250 rpm milling speed and weight ratio of the milling balls to the material 10:1. Phase identification of the powders was done on the base of x-ray diffraction patterns. They were measured using X'Pert Pro diffractometer equipped with Cu radiation. Diffractograms were registered in a step-scan mode, in 2θ angular range from 25° to 130° with step of 0.04°. Microstructure was observed using transmission electron microscope (TEM) with the high-resolution mode (HRTEM)—JEM 3010 (JEOL) operated at 300 kV.

Crystallization process was studied from measurements done using differential scanning calorimeter (DSC)—Mettler Toledo DSC 1. Samples weighted about 20–30 mg. In order to determine crystallization temperature as well as activation energy, non-isothermal studies were done. Samples were heated up from 20 to 600 °C at heating rates of 5, 10, 15, 20, 30 and 40 K/min under ambient atmosphere. Temperatures: onset— T_s , end— T_e were determined from the intersection of the tangent, drawn to the slope of the peak, with the baseline. In order to determine activation energy of crystallization, two approaches were used: Kissinger (Ref 9) and Ozawa (Ref 10). In order to

carry out phase identification, the crystallized alloys were studied using x-ray diffraction. All samples, regardless of the heating rate applied during DSC test, showed the same phase composition.

3. Results and Discussion

Figure 1 (top) shows x-ray diffraction patterns measured for freely mixed powders used as a starting mixture for the high-energy ball milling. The patterns consisted from diffraction lines characteristic for individual elemental powders. After 100 h of grinding in the high-energy ball mill (HEBM), the powders were alloyed. This was confirmed from the measured

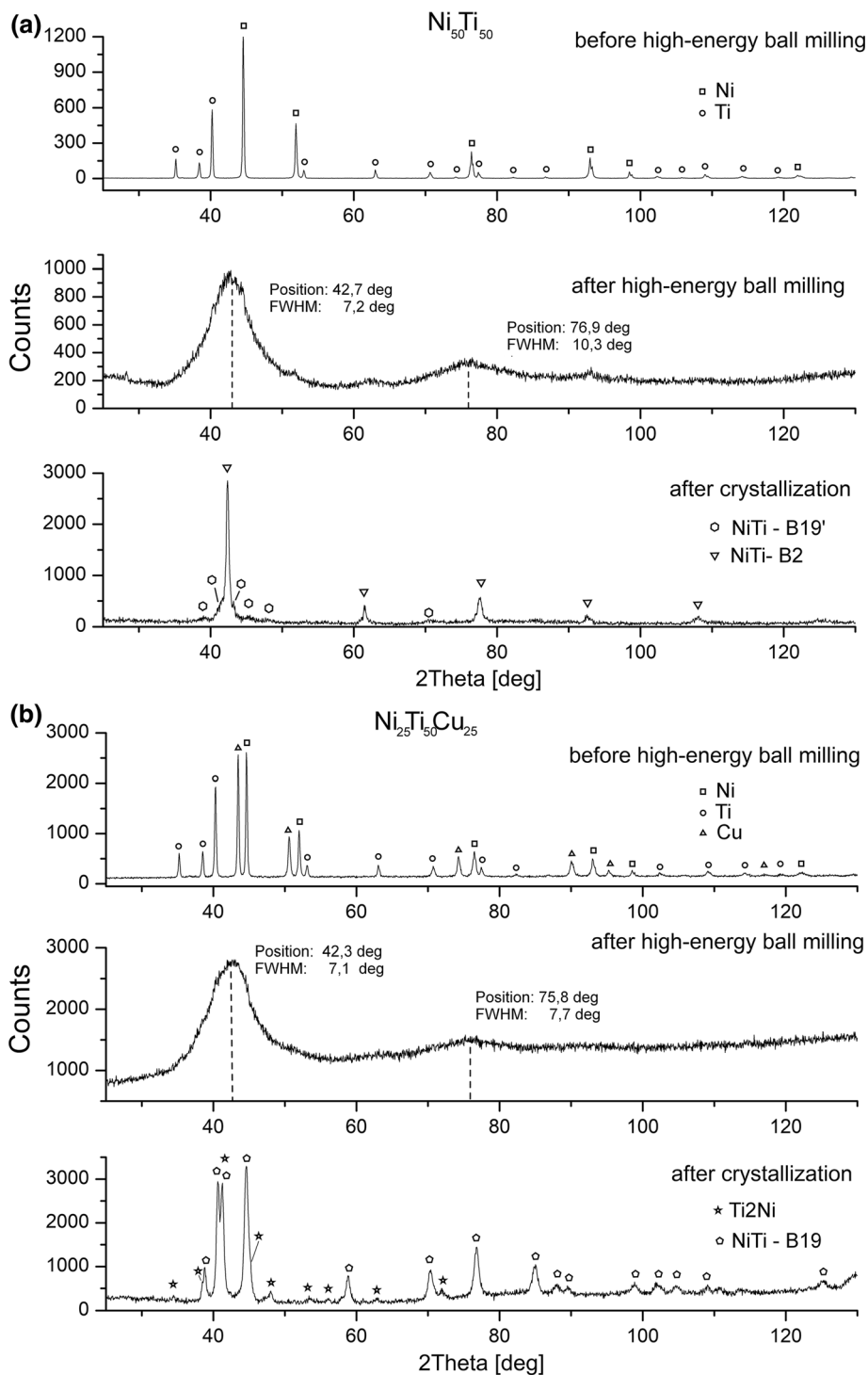


Fig. 1 X-ray diffraction patterns measured for $\text{Ni}_{50}\text{Ti}_{50}$ (a) and $\text{Ni}_{25}\text{Ti}_{50}\text{Cu}_{25}$ (b) samples: before and after of high-energy ball milling as well as after crystallization

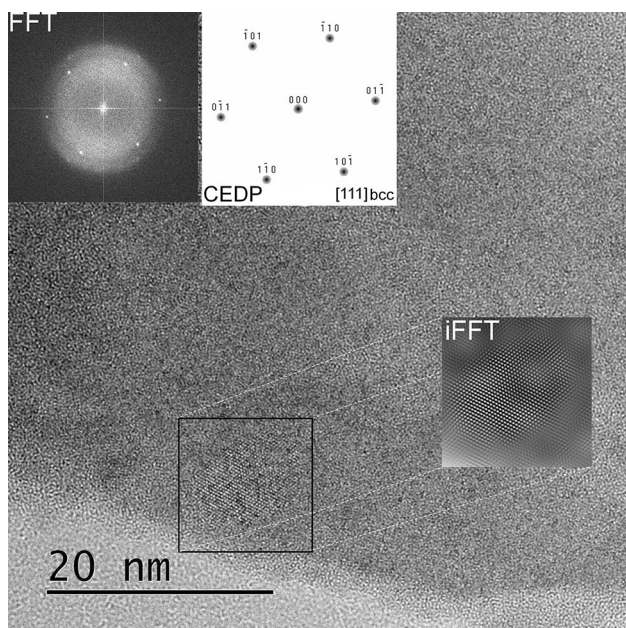


Fig. 2 HRTEM image observed for the Ni₅₀Ti₅₀ alloy milled 100 h, where FFT, fast Fourier transformation; CEDP, calculated electron diffraction pattern; iFFT, inverse fast Fourier transformation

diffractograms (Fig. 1—middle). Diffraction lines from individual alloying elements disappeared, and instead of them two diffused maxima appeared. The extended value of the full width at half maximum (FWHM) indicated the presence of an amorphous phase in both alloys. However, detailed observations carried out using the HRTEM technique revealed that, in addition to the amorphous phase, nanocrystalline regions were formed (Ref 11).

Figure 2 shows an example of HRTEM image observed for the Ni₅₀Ti₅₀ alloy milled for 100 h. Similar images were observed for the Ni₂₅Ti₅₀Cu₂₅ alloy. It can be seen that large part of the volume is amorphous, in which the nanocrystalline particles of the bcc phase were formed. After annealing, done at temperature above 777 K, in both alloys the crystalline state was confirmed from XRD studies in both alloys (Fig. 1—bottom). In the case of the crystallized Ni₅₀Ti₅₀, the presence of the B2 parent phase was identified. In addition, a small amount of the B19' monoclinic martensite was found. Due to the fact that the Ni₂₅Ti₅₀Cu₂₅ alloy shows the presence of B2-B19 martensitic transformation, at range of temperatures between 310 and 350 K, the B19 orthorhombic martensite was identified. Also, an amount of the Ti₂Ni equilibrium phase was present in the alloy.

In order to characterize crystallization process, the DSC heating curves were measured with different heating rates. Results are shown in Fig. 3. From the measured thermograms, characteristic temperatures of the crystallization peak were determined. In general, both alloys revealed similar thermal behavior. Regardless of the heating rate, on the thermograms, there was a single crystallization peak in the temperature range from 777 to 821 K and from 758 to 827 K for the Ni₅₀Ti₅₀ and Ti₅₀Ni₂₅Cu₂₅ alloys, respectively. As the heating rate increased, the characteristic temperatures for crystallizations peak increased their values. The introduction of 25 at% of copper, instead of the nickel into the alloy, lowered the crystallization temperature of about 18 degrees with respect to the binary

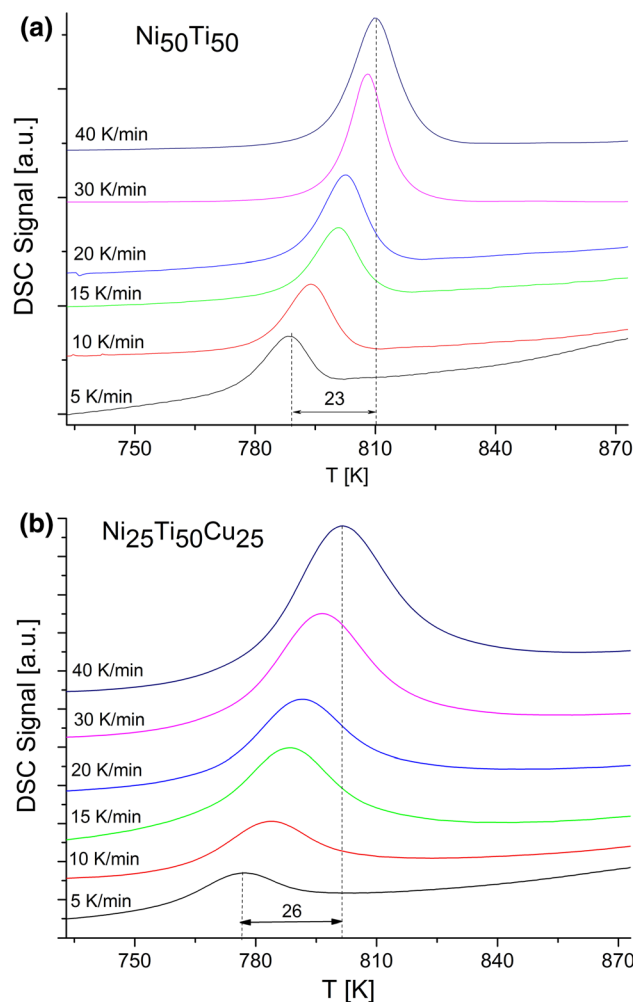


Fig. 3 The DSC heating curves measured for Ni₅₀Ti₅₀ (a) and Ti₅₀Ni₂₅Cu₂₅ samples studied at different heating rates

alloy. In contrast, the temperature of the end of crystallization for both alloys showed similar values. Moreover, the temperature range of the crystallization process was wider in the case of the Ti₅₀Ni₂₅Cu₂₅ alloy in comparison with the Ni₅₀Ti₅₀ of about 20 degrees. In both alloys, its value increased depending on the increase in the heating rate. Also significant parameter of the transformations is an enthalpy, which in the case of a ternary alloy (depending on the heating rate ranged from 71 to 78 J/g) was almost twice as high as for a binary alloy (from 33 to 38 J/g). However, the most important parameter, from the point of view of determining the activation energy, was the peak temperature. The crystallization peak temperature T_p ranged from 788 K at slowest heating rate to 813 K for the fastest one in the Ni₅₀Ti₅₀ alloy. Similar behavior has been observed for the Ti₅₀Ni₂₅Cu₂₅ alloy. Value of the peak temperature increased from 777 K at heating rate of 5 K/min to 802 K at 40 K/min.

Using data obtained from the measured DSC heating curves, the Kissinger and Ozawa plots were prepared. From slope of the $\ln(\beta/T_p^3)$ or $\ln(\beta)$ versus $1/T$ plot (Fig. 4), the activation energy (E_a) was determined (β —heating rate; T_p temperature at maximum of a thermal peak). Activation energy calculated for the Ni₅₀Ti₅₀ alloys was 410 kJ/mol (Kissinger) and 424 kJ/mol (Ozawa), for the Ti₅₀Ni₂₅Cu₂₅ alloy: 415 and 429 kJ/mol,

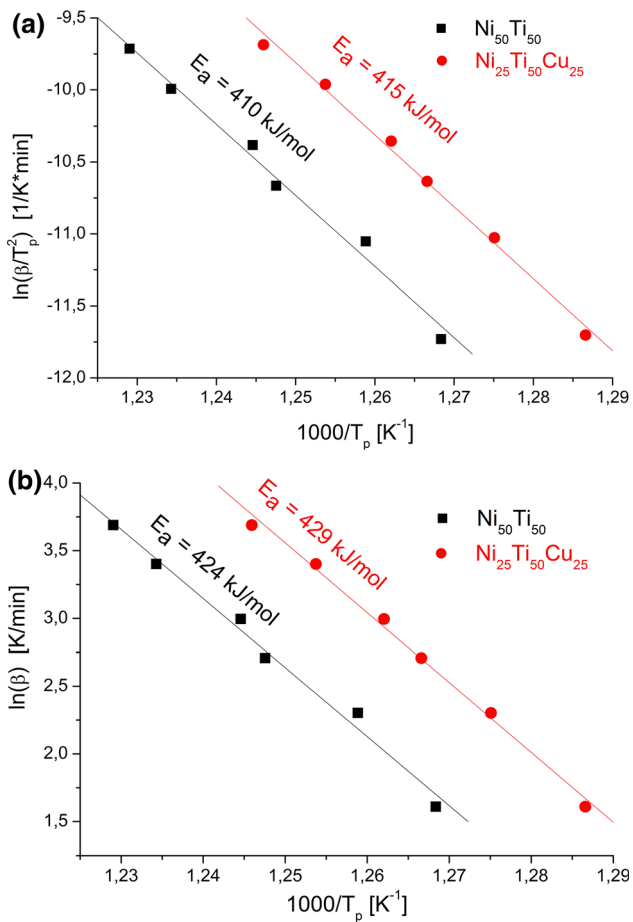


Fig. 4 The Kissinger (a) and Ozawa (b) plots for the $\text{Ti}_{50}\text{Ni}_{50}$ and $\text{Ti}_{50}\text{Ni}_{25}\text{Cu}_{25}$ alloys

respectively. Regardless of the applied calculation model, the determined values of the activation energy values are comparable. Slightly lower energies were obtained for the $\text{Ni}_{50}\text{Ti}_{50}$ alloy. It results from the lower crystallization temperatures (determined for the same heating rates) of the $\text{Ti}_{50}\text{Ni}_{25}\text{Cu}_{25}$ alloy in relation to the $\text{Ni}_{50}\text{Ti}_{50}$. This fact indicates a greater influence of the alloying technology on activation energy than the difference in a chemical composition of alloys. The key role plays the state of internal stresses and accumulated energy resulted in the increased number of structural defects such as dislocations and/or grain boundaries modified during manufacturing process. This dependence can be traced from the literature data listed in Table 1. For the binary NiTi alloys (with chemical composition close to equiatomic one) processed by heavy plastic deformation methods (HPD), such as cold rolling or high-pressure torsion, values of the activation energy range from 259 to 285 kJ/mol. It should be remembered that in the alloys processed by HPD, not all of the volume goes into an amorphous state. Depending on the HPD technique, some of the material remains in the nanocrystalline or ultrafine grains (Ref 2, 4, 12). In addition, the crystalline regions are strongly defected, which contributes to the increase in the internal state of stress and hence, the state of the stored energy. Completely different behaviors can be found in the alloys produced by magnetron sputtering (Ref 13-15). They are completely amor-

phous. Values of the activation energy are much higher and range from 403 to 416 kJ/mol. This means that their ability to crystallization is less than alloys processed by HPD methods. Gasperini et al., (Ref 16) basing on his results obtained from studies done on similar NiTi alloy manufactured by mechanical alloying (different proportions of ball to powder—5:1 and during shorter milling time), reported that $E_c = 277$ kJ/mol. This lower value of activation energy can be attributed to slightly different methodology of obtaining amorphous $\text{Ni}_{46}\text{Ti}_{54}$ alloy (wg%), introducing more internal stresses contributing to receiving less stable amorphous phase. In the case of NiTiCu alloys, which were produced by melt-spinning technique, the authors (Ref 12, 17, 18) obtained completely amorphous ribbons. Thus, the activation energy ranged from 350 to 406 kJ/mol. These discrepancies can be a result of the cooling rate realized in the melt spinning, which may affect in inhomogeneity of the chemical composition. The values of activation energy obtained in our research are comparable to alloys that exhibit the presence of the amorphous phase and require higher activation energy for crystallization. This may mean that extending of the grinding time up to 100 h leads to amorphisation and a decrease in internal stresses. It has been known from the literature that, in high-energy ball mills, during the collision of the balls with the material, the temperature is increased locally—even to receiving melting effect at the particle interface (Ref 19, 20). This may facilitate diffusion transport of alloying elements and contributes to the dynamic recovery of deformed particles.

4. Summary

The use of high-energy ball milling, with an extended grinding time to 100 h, enabled to obtain both the $\text{Ti}_{50}\text{Ni}_{50}$ and $\text{Ti}_{50}\text{Ni}_{25}\text{Cu}_{25}$ alloys in an amorphous form with few crystallized nano-areas. Despite the differences in the chemical composition of the alloys, they revealed similar values of activation energy. The ongoing process of crystallization requires activation energy of approximately 410 kJ/mol. Such a relatively high value of energy proves the high stability of the amorphous phase. In general, initiation of the crystallization process requires raising the temperature above 777 K.

Open Access

This article is licensed under a Creative Commons Attribution 4.0 International License, which permits use, sharing, adaptation, distribution and reproduction in any medium or format, as long as you give appropriate credit to the original author(s) and the source, provide a link to the Creative Commons licence, and indicate if changes were made. The images or other third party material in this article are included in the article's Creative Commons licence, unless indicated otherwise in a credit line to the material. If material is not included in the article's Creative Commons licence and your intended use is not permitted by statutory regulation or exceeds the permitted use, you will need to obtain permission directly from the copyright holder. To view a copy of this licence, visit <http://creativecommons.org/licenses/by/4.0/>.

Table 1 Crystallization parameters (E_a – Kissinger model) determined for $Ti_{50}Ni_{50}$ and $Ti_{50}Ni_{25}Cu_{25}$ alloys (where: MA, mechanical alloying; CR, cold rolling, HPT, high-pressure torsion, MS, magnetron sputtering, MSP, melt spinning)

Chemical composition	β [K/min]	T_p [K]	E_a Kissinger[kJ/mol]	E_a Ozawa[kJ/mol]	Form of material	Production method	References
$Ni_{46}Ti_{54}$	5	715	277	...	Powder	MA	(Ref 16)
	40	747					
$Ni_{50.26}Ti_{49.74}$	10	629	262	...	Bulk	CR	(Ref 12)
	40	646					
$Ni_{50.1}Ti_{49.9}$	30	648	285	...	bulk	CR	(Ref 2)
$Ni_{50.0}Ti_{50.0}$	20	648	259	...	bulk	HPT	(Ref 4)
	50	660					
$Ti_{48.99}Ni_{51.01}$	10	768	403	...	Thin film	MS	(Ref 13)
	40	784					
$Ti_{49.93}Ni_{50.07}$	5	750	416	...	Thin film	MS	(Ref 14)
	50	775					
$Ni_{50.54}Ti_{49.46}$	5	808	411	...	Thin film	MS	(Ref 15)
	40	836					
$Ni_{50.0}Ti_{50.0}$	5	788	410	415	Powder	MA	Own results
	40	810					
$Ni_{45}Ti_{50}Cu_5$	10	738	302	...	Thin film	MS	(Ref 21)
$Ni_{40.09}Ti_{49.96}Cu_{9.95}$	5	774	388	...	Thin film	MS	(Ref 14)
	50	802					
$Ni_{25}Ti_{50}Cu_{25}$	50	747	350	...	Ribbon	MSP	(Ref 16)
$Ni_{25}Ti_{50}Cu_{25}$	374	...	Ribbon	MSP	(Ref 17)
$Ni_{25}Ti_{50}Cu_{25}$	5	721	406	...	Ribbon	MSP	(Ref 18)
	40	746					
$Ni_{25}Ti_{50}Cu_{25}$	5	777	415	429	Powder	MA	Own results

References

- M. Çelikkbilek, A. Erçin and S. Aydın, Crystallization Kinetics of Amorphous Materials, Advances in Crystallization Processes, Yitzhak Mastai, InTech, 2012, p. 127-162
- M. Peterlechner, J. Bokeloh, G. Wilde, and T. Waitz, Study of relaxation and crystallization kinetics of NiTi made amorphous by repeated cold rolling, *Acta Mater.*, 2010, **58**(20), p 6637–6648
- S.Y. Jiang, M. Tang, Y.N. Zhao, L. Hu, Y.Q. Zhang, and Y.L. Liang, Crystallization of amorphous NiTi shape memory alloy fabricated by severe plastic deformation, *Trans. Nonferrous Met. Soc. China*, 2014, **24**(6), p 1758–1765
- M. Peterlechner, T. Waitz, and H.P. Karnthaler, Nanocrystallization of NiTi shape memory alloys made amorphous by high-pressure torsion, *Scr. Mater.*, 2008, **59**(5), p 566–569
- S. Chang, S. Wu, and H. Kimura, Crystallization kinetics of $Ti_{50}Ni_{25}Cu_{25}$ melt-spun amorphous ribbons, *Mater. Trans.*, 2006, **47**(10), p 2489–2492
- E. Sakher, N. Loudjani, M. Benchiheb, and M. Bououdina, Influence of Milling Time on Structural and Microstructural Parameters of $Ni_{50}Ti_{50}$ Prepared by Mechanical Alloying Using Rietveld Analysis, *J. Nanomater.*, 2018, vol. 2018
- A. Takasaki, Mechanical alloying of the Ti-Ni system, *Phys. Status Solidi A*, 1998, **162**(2), p 183–192
- B. Tian, Y.X. Tong, F. Chen, Y. Liu, and Y.F. Zheng, Phase transformation of NiTi shape memory alloy powders prepared by ball milling, *J. Alloys Compd.*, 2009, **477**(1–2), p 576–579
- H.E. Kissinger, Reaction kinetics in differential thermal analysis, *Anal. Chem.*, 1957, **29**(11), p 1702–1706
- G.K. Matusita and S. Sakka, Kinetic study on non-isothermal crystallization of glass by thermal analysis, *Bull. Inst. Chem. Res.*, 1981, **59**(3), p 159–171
- P. Salwa and T. Goryczka, Influence of milling time on formation of NiTi alloy produced by high-energy ball milling, *Arch. Metall. Mater.*, 2019, **64**(3), p 1017–1022
- K. Inaekyan, V. Brailovski, S. Prokoshkin, A. Korotitskiy, and A. Glezer, Characterization of amorphous and nanocrystalline Ti–Ni-based shape memory alloys, *J. Alloys Compd.*, 2009, **473**(1–2), p 71–78
- Y.C. Lei, W. Cai, X. An, and L.X. Gao, The effect of the underlying substrate on crystallization kinetics of TiNi thin films, *J. Non-Cryst. Solids*, 2008, **354**(40), p 4572–4576
- J.Z. Chen and S.K. Wu, Crystallization temperature and activation energy of rf-sputtered near-equiatom TiNi and $Ti_{50}Ni_{40}Cu_{10}$ thin films, *J. Non-Cryst. Solids*, 2001, **288**(1–3), p 159–165
- K.T. Liu and J.G. Duh, Kinetics of the crystallization in amorphous NiTi thin films, *J. Non-Cryst. Solids*, 2007, **353**(11–12), p 1060–1064
- A.A.M. Gasperini, K.D. Machado, S. Buchner, J.C. de Lima, and T.A. Grandi, Influence of the temperature on the structure of an amorphous $Ni_{46}Ti_{54}$ alloy produced by mechanical alloying, *Eur. Phys. J. B*, 2008, **64**(2), p 201–209
- P. Schlossmacher, N. Boucharat, H. Rösner, and A.V. Shelyakov, Crystallization studies of amorphous melt-spun $Ni_{25}Ti_{50}Cu_{25}$, *J. Phys. IV France*, 2003, **112**, p 731–734
- Y. Tong and Y. Liu, Crystallization behavior of a $Ti_{50}Ni_{25}Cu_{25}$ melt-spun ribbon, *J. Alloys Compd.*, 2008, **449**(1–2), p 152–155
- M. Atzmon, In situ thermal observation of explosive compound-formation reaction during mechanical alloying, *Phys. Rev. Lett.*, 1990, **64**(4), p 487–490
- C.C. Koch, Synthesis of nanostructured materials by mechanical milling: problems and opportunities, *Nanostruct. Mater.*, 1997, **9**, p 13–22
- M. Mohri, M. Nili-Ahmadabadi, V. Sai, and K. Chakravadhanula, Crystallization study of amorphous sputtered NiTi bi-layer thin film, *Mater. Charact.*, 2015, **103**, p 75–80

Publisher's Note Springer Nature remains neutral with regard to jurisdictional claims in published maps and institutional affiliations.